Chemistry–A European Journal
Research Article
doi.org/10.1002/chem.202400187
Chemistry Europe
European Chemical Societies Publishing
www.chemeurj.org

Real-Time Metabolic Magnetic Resonance Spectroscopy of Pancreatic and Colon Cancer Tumor-Xenografts with Parahydrogen Hyperpolarized 1-^{13}C Pyruvate-d_3

Lisa M. Fries[+],[a, b] Theresa L. K. Hune[+],[a, b] Sonja Sternkopf[+],[a, b] Salvatore Mamone,[a, b, f] Kim Lucia Schneider,[c, d] Ramona Schulz-Heddergott,[c, d] Dorothea Becker,[e] and Stefan Glöggler*[a, b]

Parahydrogen-induced polarization (PHIP) is an emerging technique to enhance the signal of stable isotope metabolic contrast agents for Magnetic Resonance (MR). The objective of this study is to continue establishing 1-^{13}C-pyruvate-d_3, signal-enhanced via PHIP, as a hyperpolarized contrast agent, obtained in seconds, to monitor metabolism in human cancer. Our focus was on human pancreatic and colon tumor xenografts. 1-^{13}C-vinylpyruvate-d_6 was hydrogenated using parahydrogen. Thereafter, the polarization of the protons was transferred to ^{13}C. Following a workup procedure, the free hyperpolarized 1-^{13}C-pyruvate-d_3 was obtained in clean aqueous solution. After injection into animals bearing either pancreatic or colon cancer xenografts, slice-selective MR spectra were acquired and analyzed to determine rate constants of metabolic conversion into lactate and alanine. 1-^{13}C-pyruvate-d_3 proved to follow the increased metabolic rate to lactate and alanine in the tumor xenografts.

Introduction

Magnetic resonance spectroscopy and imaging is a powerful, non-invasive tool widely applied in medical diagnostics, but a limitation is its low sensitivity.[1] To overcome this limitation, signal-enhancement or hyperpolarization techniques were introduced to increase MR signals by more than four orders of magnitude.[2] This technique complements Positron Emission Tomography (PET)[3] that can locate premalignant lesions and tumors, but cannot reveal metabolic activity inside premalignant lesions and tumors.[4] The development of hyperpolarization methods makes it possible to enhance the signals of ^{13}C-enriched metabolites, such as pyruvate, and to follow directly its downstream metabolites and thereby, providing information regarding metabolic changes in disease.[3a,5] Pyruvate is a metabolite that has a key role in cellular metabolism. In healthy tissue, pyruvate dehydrogenase facilitates the decarboxylation of pyruvate and thereby gives access to the tricarboxylic acid (TCA) cycle. Alternatively, pyruvate can undergo conversion by alanine aminotransferase to alanine or reduction by lactate dehydrogenase into lactate.[6] The production of lactate under aerobic conditions is a hallmark of many malignancies, a phenomenon commonly referred to as the Warburg effect.[7] The most prominent primary technique for real-time metabolic investigations is Dynamic Nuclear Polarization (DNP), which has led to noticeable advances regarding studies of human malignancies by way of hyperpolarizing pyruvate and to detect, in real time, the Warburg effect.[8] However, in part due to its complexity and, not infrequently, long wait times regarding the production of metabolic contrast agents, the clinical application of this technique is not always effortless.[9] Enhancement techniques based upon parahydrogen, which are scalable and fast, have recently made possible the hyperpolarization of metabolites within seconds rather than tens of minutes to hours compared to DNP.[5c,10] The PHIP-SAH (parahydrogen induced polarization-side arm hydrogenation) facilitates the development of numerous novel contrast agents, such as pyruvate. The introduction of double bonds to the molecule by a sidearm, which can be cleaved, expands the possibilities to monitor metabolic processes.[5c]

[a] L. M. Fries,[+] T. L. K. Hune,[+] S. Sternkopf,[+] S. Mamone, S. Glöggler
NMR Signal Enhancement Group Max Planck Institute for Multidisciplinary Sciences, Am Faßberg 11, 37077 Göttingen, Germany
E-mail: Stefan.gloeggler@mpinat.mpg.de

[b] L. M. Fries,[+] T. L. K. Hune,[+] S. Sternkopf,[+] S. Mamone, S. Glöggler
Center for Biostructural Imaging of Neurodegeneration, University Medical Center Göttingen, Robert-Koch-Straße 40, 37075 Göttingen, Germany

[c] K. L. Schneider, R. Schulz-Heddergott
Department of Molecular Oncology, , University Medical Center Göttingen, Justus von Liebig Weg 11, 37077 Göttingen, Germany

[d] K. L. Schneider, R. Schulz-Heddergott
Clinical Research Unit 5002, University Medical Center Göttingen, Robert-Koch-Straße 40, 37075 Göttingen, Germany

[e] D. Becker
Department of NMR-based Structural Biology, Max Planck Institute for Multidisciplinary Sciences, Am Faßberg 11, 37077 Göttingen, Germany

[f] S. Mamone
Present address: Department of Life, Health and Environmental Science, University of L'Aquila, Via Vetoio, Localita' Coppito, 67100, L'Aquila, Italy.

[+] These authors contributed equally to the work, names listed in alphabetical order.

Supporting information for this article is available on the WWW under https://doi.org/10.1002/chem.202400187

In a previous study,[10c] we introduced 1-^{13}C-pyruvate-d_3 to monitor the metabolism of human derived melanoma xenografts in mice with non-localized ^{13}C-spectroscopy. Deuteration of the molecule prolonged T_1 relaxation and increased values of hyperpolarization and therefore improved its suitability for magnetic resonance investigations. The objective of the study presented here is to establish 1-^{13}C-pyruvate-d_3, enhanced via parahydrogen, as a probe for additional malignancies apart from melanoma. In this proof-of-concept study we demonstrate its feasibility to differentiate between pyruvate conversion rates using slice-selective ^{13}C-spectroscopy. Here, we observed the perdeuterated ^{13}C-pyruvate metabolism of mice with either pancreatic or colon cancer tumor-xenografts. Colon cancer is the second most deadly cancer due to its high and growing incidence numbers.[11] Pancreatic cancer is one of the leading cancer-related death causes worldwide, in part due to few signs and symptoms in its early-stages of development.[12] Therefore, in the case of pancreatic cancer, having contrast agents available that can detect this very aggressive and as yet incurable malignancy in its early stages would be a significant advance.[13] Both pancreatic[4a,8a,d] and colon cancer[8c,14] have been studied with hyperpolarized pyruvate generated by DNP, identifying it as a promising probe to monitor metabolism in these cancer types. To the best of our knowledge, our study is the first to apply 1-^{13}C-pyruvate-d_3 in particular hyperpolarized with parahydrogen to investigate these two cancer types, aimed at establishing methodologies for early and differential diagnosis.

Results and Discussion

Results

The aim of this study was to continue the investigation of the feasibility of hyperpolarized 1-^{13}C-pyruvate-d_3 to evaluate pyruvate conversion rates of different malignancies and to show potential differences. Therefore, the hyperpolarization was quantified directly after the transfer from ^{1}H to ^{13}C via the MINERVA pulse sequence of the precursor 1-^{13}C-vinylpyruvate-d_6 at 53 ± 2%. Following the requisite procedures for sample preparation and polarization, the resultant polarization level of the injection-ready sample was observed to be 12 ± 4%. In both types of the human tumor-xenografts, pyruvate was converted quickly to lactate and alanine. (Figure 1, pyruvate signal appears at 171.1 ppm, the alanine signal at 176.8 ppm and the lactate signal at 183.3 ppm). In the pancreatic tumor-xenografts, alanine was already at its maximum at the start of the measurement and thus, only an increase in lactate was detected (Figure 2A). In the colon tumor-xenografts, two of the three mice showed also the increase of alanine signal (Figure 2B).

Furthermore, area-under-the-curve (AUC) ratios of the metabolites and their conversion rates are important parameters for treatment response. Table 1 shows the resulting ratios of lactate to pyruvate (Lac/Pyr) and alanine to pyruvate (Ala/Pyr) derived from the AUC model as well as the resulting rate constants k_{PL} and k_{PA} for the two entities. There is a trend that

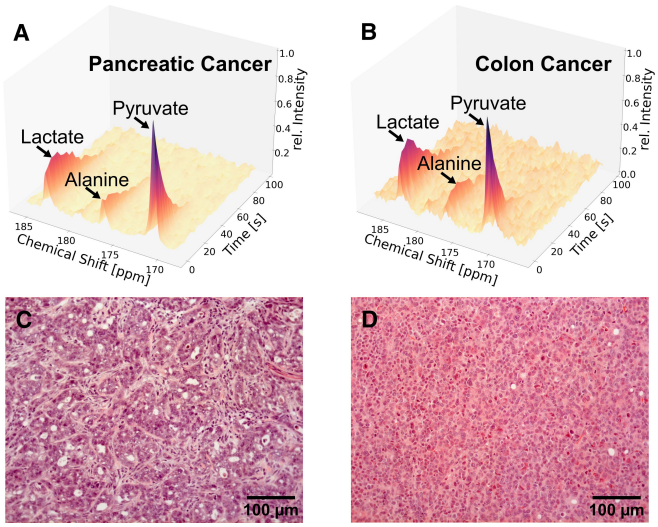

Figure 1. ^{13}C NMR spectra upon injection of hyperpolarized 1-^{13}C-pyruvate-d_3 into a mouse bearing pancreatic (A) or colon cancer (B) tumor-xenografts. The pyruvate signal appears at 171.1 ppm, the alanine signal at 176.8 ppm and the lactate signal at 183.3 ppm. The spectra were acquired 15 s after injection, every 3 s with a flip angle of 22°. Signals were normalized to the highest intensity. Tissue sections from a pancreatic (C) and a colon cancer tumor-xenograft (D) were stained with H&E.

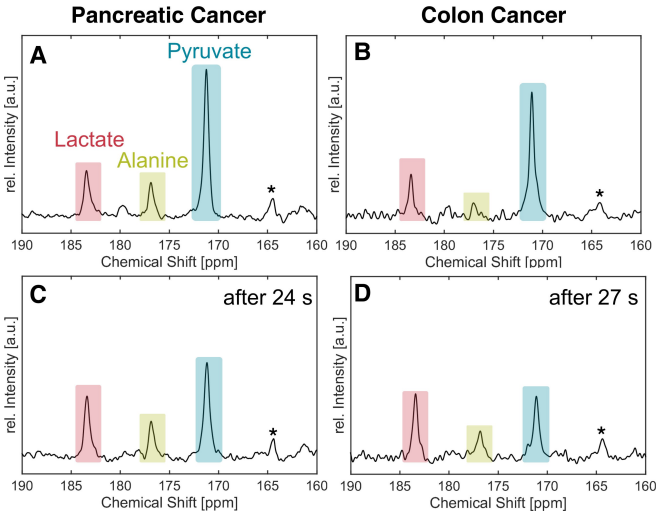

Figure 2. 1D ^{13}C NMR spectra of maximal pyruvate and lactate signals of a mouse bearing a pancreatic tumor-xenograft (A,C) and of a mouse bearing a colon cancer tumor-xenograft (B,D). A,B: Maximal pyruvate signal 15 s after injection of pyruvate into a mouse bearing a pancreatic tumor-xenograft (A) and into a mouse bearing a colon cancer tumor-xenograft (B). C: Maximal lactate signal 24 s after injection into pancreatic tumor-xenograft. D: Maximal lactate signal 27 s after injection into colon cancer tumor-xenograft. The pyruvate signal (blue) is at 171.1 ppm, the alanine signal (green) at 176.8 ppm and the lactate signal (red) at 183.3 ppm. The signal marked with an asterisk is from a urea reference.

Table 1. Metabolic ratios and conversion rates of pancreatic and colon cancer tumor-xenograft. Results are presented as mean values (n = 3) with standard deviation.

Cancer	AUC Lac/Pyr	AUC Ala/Pyr	k_{PL} [s^{-1}]	k_{PA} [s^{-1}]
Pancreatic	1.0 ± 0.2	0.5 ± 0.1	0.05 ± 0.01	0.035 ± 0.004
Colon	1.7 ± 0.6	0.7 ± 0.1	0.08 ± 0.03	0.05 ± 0.01

in human colon cancer tumor-xenografts the ratios lactate to pyruvate (Lac/Pyr) and alanine to pyruvate (Ala/Pyr) derived from the AUC model were slightly higher than in human pancreatic cancer-xenografts. Figure 3A and B illustrate variability in individual measurements.

Since we see a trend of higher metabolic rates with larger tumor volumes examined by anatomical ^{1}H images (Supp Table S1, Supp Figures S3 and S4), we propose a potential correlation between metabolic activity and tumor volume. As normalization on tumor volume has been performed in the literature before, we decided to normalize it which resulted in smaller variation.[4b] In detail, we propose a normalization with tumor volume, by assuming an ellipsoidal shape,[15] (Supplementary Table S1) obtained from the anatomical proton images (Supplementary Figures S3 and S4).[4b] Figure 3C and D show the data after normalization. The correlated data showed smaller scattering, the results are summarized in Table 2.

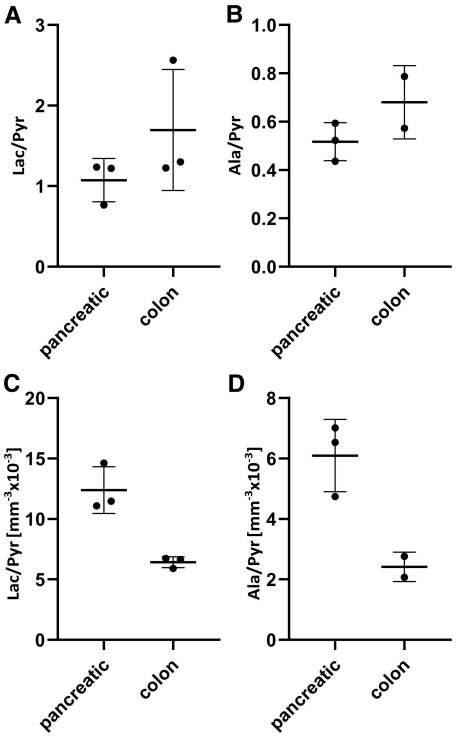

Figure 3. Plots of (A) Lac/Pyr ratio and (B) k_{PL} Ala/Pyr ratio of pancreatic (n = 3) and colon cancer tumor-xenografts including mean and standard deviation (n = 3 for Lac/Pyr ratio and n = 2 for Ala/Pyr ratio). Plots of Lac/Pyr ratio (C) and k_{PA} Ala/Pyr ratio (D) of pancreatic (n = 3) and colon cancer tumor-xenografts correlated with tumor size including mean and standard deviation.

Discussion

Three mice, bearing bilaterally, human pancreatic tumor-xenografts and likewise, three mice, bearing bilaterally, human colon cancer tumor-xenografts, were injected with a single dose of hyperpolarized 1-^{13}C-pyruvate-d_3 solution. From hyperpolarizing the probe until injection it took less than two minutes. In comparison to DNP, which requires at least 10 min and at times, several hours per dose of hyperpolarized pyruvate,[9] the technique and its application described here, is significantly faster and allows multiple or semi-continuous injection of pyruvate.[10c] In a study by Serrao et al.,[8d] it was shown that MRI with hyperpolarized 1-^{13}C-pyruvate detects advanced pancreatic preneoplasia prior to invasive disease in a mouse model. While those results were obtained with pyruvate hyperpolarized with dissolution DNP, our real-time MRS was carried out with parahydrogen hyperpolarized 1-^{13}C pyruvate-d_3 with no substantial effects of deuteration of pyruvate.[16] However, comparison of absolute conversion rate values remains challenging, due to many differences regarding experimental protocol in between PHIP and DNP studies. As we envisioned in our introductory study of this molecule,[10c] we were able to show differences regarding the metabolism between two different types of human tumor-xenografts. We suggest a normalization between the lactate/pyruvate (Lac/Pyr) and alanine/pyruvate (Ala/Pyr) ratios with tumor volume, as individual data points converge. This relationship has been previously documented in the literature for human breast cancer patients.[4b] However, a study in canine cancer patients with sarcoma did not point to a correlation between tumor volume and the kinetic parameter k_{PL}.[17] It is difficult to extrapolate from this published study, pursued in tumors arising in dogs, insights into this correlation with human tumor xenografts. Our data, shown herein, suggest that the higher metabolic activity we detected in the human pancreatic tumor-xenografts versus in the human colon cancer tumor-xenografts might be a promising approach regarding early detection of these two malignancies.

Furthermore, differences among cell lines of a given malignancy could potentially be detected by comparative analysis of distinct metabolic conversion rates and thus promising a route for differential diagnostics. In this proof-of-concept study, we acquired a non-localized ^{13}C-spectrum after the completion of injection, to ensure pyruvate arrival in the animal. Directly afterwards, the acquisition of slice-selective spectra followed. In this way, we had more control over the injection, but at the same time lost the first temporal points of the metabolites' kinetic curves. This can be a possible source of variation, which is reduced by the fact that for each animal, the

Table 2. Metabolic ratios and conversion rates of pancreatic and colon cancer tumor-xenografts normalized by tumor volume. Results are presented as mean values (n = 3) with standard deviation.

Cancer	AUC Lac/Pyr [mm^{-3}]×10^{-3}	AUC Ala/Pyr [mm^{-3}]×10^{-3}	k_{PL} [s^{-1} mm^{-3}]×10^{-3}	k_{PA} [s^{-1} mm^{-3}]×10^{-3}
Pancreatic	12 ± 2	6 ± 1	0.62 ± 0.08	0.41 ± 0.07
Colon	6.4 ± 0.4	2.4 ± 0.4	0.32 ± 0.02	0.16 ± 0.02

time between injection and slice-selective acquisition start was the same. Rather than acquiring a spectrum over the entire tumor volume, acquiring images or spectra of different parts of tumors with single-voxel spectroscopy or CSI might detect subtle differences in the tissue of tumors of a same malignancy in the future. As a proof-of-concept study, the results presented here motivate to continue the investigations with a larger panel of PDAC and CRC xenografts harboring different cancer cell lines.

Conclusions

We provide the first experimental evidence that 1-^{13}C-pyruvate-d_3, hyperpolarized within seconds via parahydrogen, can be used to monitor the metabolism of human pancreatic and colon cancer tumor-xenografts. We envision that rapidly hyperpolarized MR can accompany PET and other tools to aid in the early diagnosis of as yet untreatable human malignancies.

Experimental Section

Materials and Instruments

All chemicals were purchased from commercial suppliers. 1-^{13}C-pyruvate-d_3 was synthesized according to our published procedure.[10d] The hyperpolarization was performed on a Bruker ultrashield 300 MHz (7.05 T) spectrometer. The in vivo experiments were acquired on a Bruker ultrashield 300 MHz (7.05 T) spectrometer (wide bore) equipped with a Bruker MicWB40 rf probe, Micro 2.5 WB gradient system and 30 mm diameter ^{1}H/^{13}C coil (Bruker MICB40 RES 300 1H/13C 040/030 QTR). The parahydrogen fraction of dihydrogen gas was enriched to $>$98% by cooling down to 20 K with a He-cooled parahydrogen generator provided by a cryocooler system (Sumimoto HC-4A helium compressor, Sumimoto Cold Head CH-204 with parahydrogen reaction chamber by ColdEdge Technologies, temperature controller Lake Shore Cryotronics, Inc.) and delivered by a home-built valve and tubing system.

Hyperpolarization

The experiments were performed in accordance with our recently introduced protocol (Figure 4) using the MINERVA (Maximizing Insensitive Nuclear Enhancement Reached Via parahydrogen Amplification) pulse sequence for polarization transfer. 70 mM of the precursor 1-^{13}C-vinylpyruvate-d_6 and 13 mM of the commercially available catalyst ([1,4-Bis(diphenyl-lphosphino)butane](1,5-cyclooctadiene)rhodium(I)tetrafluoro-borate) were dissolved in acetone-d_6. Parahydrogen gas was supplied to 200 µl of the degassed solution for 20 s with a pressure of 7 bar at 330 K. After the polarization transfer to the 1-^{13}C-carbon using MINERVA, the cleavage of the sidearm was performed by adding 75 µl of 150 mM Na_2CO_3 in H_2O solution. After 2 s of mixing by nitrogen gas and 0.5 s of settling time, acetone-d_6 was evaporated through a vacuum pump for 10 s at 323 K in a heated water bath outside the spectrometer. The pH of the solution was adjusted to physiological conditions ~7.4 pH by adding 75 µl of 100 mM HEPES buffer with pH 3. The solution was filtered (1.2 µm pore size) and immediately transferred to the MRI spectrometer. Residual rhodium and acetone content is reduced to far below toxic levels, as established previously.[10d] For injection, a catheter containing a T-piece was used: The sodium chloride solution inside the catheter was drained out of the system through one output, resulting in injection of pure hyperpolarized pyruvate solution.

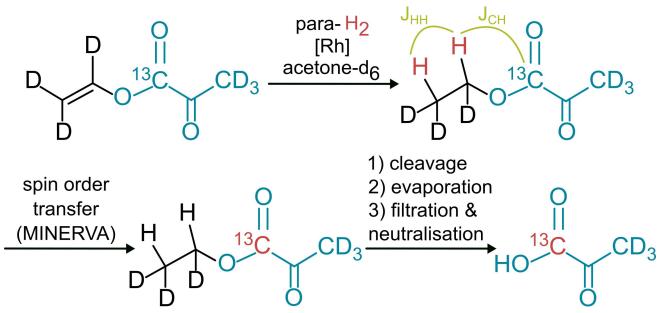

Figure 4. Synthesis of 1-^{13}C-pyruvate-d_3 and MINERVA protocol for hyperpolarization. The sidearm of the molecule is shown in black, the final product in blue, and the hyperpolarized nuclei are marked in red. The precursor 1-^{13}C-vinylpyruvate-d_6 and the rhodium-catalyst were dissolved in acetone-d_6 and parahydrogen gas was supplied. Following the polarization transfer to 1-^{13}C using MINERVA, the cleavage of the sidearm was performed. Acetone-d_6 was evaporated and the pH of the solution was adjusted to physiological conditions.

Imaging and Spectroscopy

To determine the location of each tumor, a coronal ^{1}H T_2-weighted RARE (Rapid Acquisition with Relaxation Enhancement) with a FOV 45×30 mm^2 and an image size of 128×128 matrix was recorded (90 slices, slice thickness 0.5 mm, detailed parameters in the SI). Thereafter, the metabolic kinetics of the pyruvate conversion were analyzed. The polarization values were determined according to the procedure described in[10c] and in the SI. 15 s after injection of the hyperpolarized pyruvate, a non-localized spectrum over the entire animal, with a flip angle of 10°, was recorded to ensure the arrival of the pyruvate. Thereafter, spectra were recorded every 3 s with a flip angle of 22° and one scan per spectrum. The spectra were localized in the tumor by way of selecting a slice of 12 mm in the axial plane (Supplementary Figure S1).

Data Analysis

Data Processing was performed with TopSpin 4.0.8. Spectra were phase corrected in the 0th and 1st order, line broadening was applied to 30 Hz and baseline correction was applied. Further analysis of the data was performed using Python 3.0 in Jupyter Notebooks. The processed data is shown in Supplementary Figure S2 in a 3D plot.

Peak Intensities were normalized to the signal of highest intensity of the respective dataset, which was always the maximum of the pyruvate resonance. Except in the case of one animal where the alanine signal was too low to analyze, integrals for the peaks of pyruvate, lactate and alanine were determined for each time point for all of the other mice.

To estimate the conversion rates from pyruvate to lactate and alanine, the area under the curve (AUC) for the injected pyruvate and the generated metabolites lactate and alanine was calculated using the above mentioned integrals. The ratio of the AUC is proportional to the forward apparent conversion constant.[8b] The following equations are derived from[8b] under the assumption that back conversion from lactate to pyruvate (k_{LP}) and alanine to pyruvate (k_{AP}) is 0 ($k_{LP} = k_{AP} = 0$).

$$\frac{AUC(L)}{AUC(P)} = \frac{k_{PL}}{R_{app}(L)} \quad (1)$$

$$\frac{AUC(A)}{AUC(P)} = \frac{k_{PA}}{R_{app}(A)} \quad (2)$$

Apparent relaxation rates $R_{app}(L)$ and $R_{app}(A)$ were calculated with estimated values for $T_1(L) = 30$ s and $T_1(A) = 20$ s and corrected for magnetization losses due to pulses with flip angle θ and repetition time TR according to Equation (3).

$$R_{app} = \frac{1}{T1} - \frac{\ln(\cos\theta)}{TR} \quad (3)$$

Results were analyzed for statistical significance using the unpaired two-tailed t-test.

Human Pancreatic and Colon Cancer Tumor-Xenografts

Carried out under approved Niedersächsisches Landesamt für Verbraucherschutz und Lebensmittelsicherheit (LAVES) protocol (20/3563), the CAPAN-2 human pancreatic and likewise, the SW480 human colon cancer cells, suspended in sterile phosphate-buffered saline, were injected subcutaneously over the right as well as the left flank of 4–5 weeks-old female nude mice (CAnN.Cg-Foxn1nu/Crl) (Charles River Laboratories, Charles River GmbH & Co. KG).

Histological Analysis

Upon completion of the imaging of the tumor-xenografts, the mice were sacrificed and their tumors resected and fixed overnight in 3.5% paraformaldehyde. Following several rinses in phosphate-buffered saline, dehydration in ethanol and infiltration of xylol, the tumor-xenografts were embedded in paraffin, sectioned and stained with Mayer's hemalum solution and eosin using standard immunohistochemical protocols. Images of the H&E stained tumor tissue sections were acquired with a Zeiss standard fluorescence microscope (Carl Zeiss AG) with the ZENblue imaging software V3.0.

Animal Housing Conditions

The BALB/c nu/nu mice were housed in the Zentrale Tierexperimentelle Einrichtung (ZTE) of the Universitätsmedizin Göttingen (UMG) Göttingen (Germany). They were housed in cages with a maximum of 5 animals per cage under standard laboratory conditions with a 12 h light cycle and with water and food available ad libitum.

Anesthesia

For initial narcosis, a solution consisting of 4 ml 0.9% sterile NaCl solution (B. Braun, Melsungen, Germany) 0.4 ml Medetomidine (1 mg/ml; Zoetis Deutschland GmbH, Berlin, Germany) and 0.6 ml Ketamine (50 mg/ml; Inresa Arzneimittel GmbH, Freiburg, Germany) was prepared. The weight of the animals was determined, followed by an intraperitoneal injection of 5 µl narcosis solution per gram body weight. Upon anesthesia of an animal, a catheter was placed into its lateral tail vein. During the time an animal was in the NMR machine, anesthesia was maintained using 1–2% Isoflurane (Baxter Deutschland GmbH, Heidelberg) in O_2 and air, which was administered via a breathing mask with a Multi Delivery System (Rothacher Medical GmbH, Heitenried, Switzerland). Breathing and temperature were monitored during the procedure using a Model 1030 MR-compatible Small Animal Monitoring and Gating System (SA Instruments Inc. New York, USA). The isoflurane level was maintained between 1–1.5%.

Supporting Information Summary

The Supporting Information includes details regarding the used pulse sequences, quantification of polarization, data analysis and tumor size determination. No additional references have been cited within the Supporting Information.

Acknowledgements

This study was supported by the Max Planck Society and funds from the European Research Council (ERC) under the European Union's Horizon 2020 research and innovation program (Grant agreement No. 949180). The Graphical Abstract was created with Biorender.com. Open Access funding enabled and organized by Projekt DEAL.

Conflict of Interests

SG is a co-founder of MagniKeen.

Data Availability Statement

The data that support the findings of this study are available in the supplementary material of this article.

Keywords: NMR · Parahydrogen · Hyperpolarization

[1] R. W. Brown, Y. C. N. Cheng, E. M. Haacke, M. R. Thompson, R. Venkatesan, *Magnetic Resonance Imaging*, **2014**, p. 1–15.
[2] a) J. H. Ardenkjaer-Larsen, B. Fridlund, A. Gram, G. Hansson, L. Hansson, M. H. Lerche, R. Servin, M. Thaning, K. Golman, *Proc. Natl. Acad. Sci. U S A* **2003**, *100*, 10158–10163; b) C. R. Bowers, D. P. Weitekamp, *J. Am. Chem. Soc.* **1987**, *109*, 5541–5542; c) J. Eills, D. Budker, S. Cavagnero, E. Y. Chekmenev, S. J. Elliott, S. Jannin, A. Lesage, J. Matysik, T. Meersmann, T. Prisner, J. A. Reimer, H. Yang, I. V. Koptyug, *Chem. Rev.* **2023**, *123*, 1417–1551; d) A. C. Pinon, A. Capozzi, J. H. Ardenkjaer-Larsen, *MAGMA* **2021**, *34*, 5–23.
[3] a) S. S. Gambhir, *Nat. Rev. Cancer* **2002**, *2*, 683–693; b) H. Gutte, A. E. Hansen, S. T. Henriksen, H. H. Johannesen, J. Ardenkjaer-Larsen, A. Vignaud, A. E. Hansen, B. Børresen, T. L. Klausen, A. M. Wittekind, N. Gillings, A. T. Kristensen, A. Clemmensen, L. Højgaard, A. Kjær, *Am. J. Nucl. Med. Mol. Imaging* **2014**, *5*, 38–45.
[4] a) H. Stodkilde-Jorgensen, C. Laustsen, E. S. S. Hansen, R. Schulte, J. H. Ardenkjaer-Larsen, A. Comment, J. Frokiaer, S. Ringgaard, L. B. Bertelsen, M. Ladekarl, B. Weber, *J. Magn. Reson. Imaging* **2020**, *51*, 961–963; b) F. A. Gallagher, R. Woitek, M. A. McLean, A. B. Gill, R. Manzano Garcia, E. Provenzano, F. Riemer, J. Kaggie, A. Chhabra, S. Ursprung, J. T. Grist, C. J. Daniels, F. Zaccagna, M. C. Laurent, M. Locke, S. Hilborne, A. Frary, T. Torheim, C. Boursnell, A. Schiller, I. Patterson, R. Slough, B. Carmo, J. Kane, H. Biggs, E. Harrison, S. S. Deen, A. Patterson, T. Lanz, Z. Kingsbury, M. Ross, B. Basu, R. Baird, D. J. Lomas, E. Sala, J. Wason, O. M. Rueda, S. F. Chin, I. B. Wilkinson, M. J. Graves, J. E. Abraham, F. J. Gilbert, C. Caldas, K. M. Brindle, *Proc. Natl. Acad. Sci. U S A* **2020**, *117*, 2092–2098; c) N.

Sushentsev, M. A. McLean, A. Y. Warren, A. J. V. Benjamin, C. Brodie, A. Frary, A. B. Gill, J. Jones, J. D. Kaggie, B. W. Lamb, M. J. Locke, J. L. Miller, I. G. Mills, A. N. Priest, F. J. L. Robb, N. Shah, R. F. Schulte, M. J. Graves, V. J. Gnanapragasam, K. M. Brindle, T. Barrett, F. A. Gallagher, *Nat. Commun.* **2022**, *13*, 466; d) S. Tang, M. V. Meng, J. B. Slater, J. W. Gordon, D. B. Vigneron, B. A. Stohr, P. E. Z. Larson, Z. J. Wang, *Cancer* **2021**, *127*, 2693–2704.

[5] a) K. M. Brindle, K. R. Keshari, *MAGMA* **2021**, *34*, 1–3; b) S. E. Day, M. I. Kettunen, F. A. Gallagher, D. E. Hu, M. Lerche, J. Wolber, K. Golman, J. H. Ardenkjaer-Larsen, K. M. Brindle, *Nat. Med.* **2007**, *13*, 1382–1387; c) F. Reineri, T. Boi, S. Aime, *Nat. Commun.* **2015**, *6*, 5858; d) K. Golman, R. in 't Zandt, M. Thaning, *Proc. Natl. Acad. Sci. U S A* **2006**, *103*, 11270–11275.

[6] L. R. Gray, S. C. Tompkins, E. B. Taylor, *Cell. Mol. Life Sci.* **2014**, *71*, 2577–2604.

[7] O. Warburg, *Science* **1956**, *123*, 309–314.

[8] a) P. Dutta, M. R. Perez, J. Lee, Y. Kang, M. Pratt, T. C. Salzillo, J. Weygand, N. M. Zacharias, S. T. Gammon, E. J. Koay, M. Kim, F. McAllister, S. Sen, A. Maitra, D. Piwnica-Worms, J. B. Fleming, P. K. Bhattacharya, *J. Proteome Res.* **2019**, *18*, 2826–2834; b) D. K. Hill, M. R. Orton, E. Mariotti, J. K. Boult, R. Panek, M. Jafar, H. G. Parkes, Y. Jamin, M. F. Miniotis, N. M. Al-Saffar, M. Beloueche-Babari, S. P. Robinson, M. O. Leach, Y. L. Chung, T. R. Eykyn, *PLoS One* **2013**, *8*, e71996; c) K. Saito, S. Matsumoto, Y. Takakusagi, M. Matsuo, H. D. Morris, M. J. Lizak, J. P. Munasinghe, N. Devasahayam, S. Subramanian, J. B. Mitchell, M. C. Krishna, *Clin. Cancer Res.* **2015**, *21*, 5073–5081; d) E. M. Serrao, M. I. Kettunen, T. B. Rodrigues, P. Dzien, A. J. Wright, A. Gopinathan, F. A. Gallagher, D. Y. Lewis, K. K. Frese, J. Almeida, W. J. Howat, D. A. Tuveson, K. M. Brindle, *Gut* **2016**, *65*, 465–475.

[9] K. Golman, R. I. Zandt, M. Lerche, R. Pehrson, J. H. Ardenkjaer-Larsen, *Cancer Res.* **2006**, *66*, 10855–10860.

[10] a) M. Goldman, H. Johannesson, O. Axelsson, M. Karlsson, *Magn. Reson. Imaging* **2005**, *23*, 153–157; b) E. Cavallari, C. Carrera, M. Sorge, G. Bonne, A. Muchir, S. Aime, F. Reineri, *Sci. Rep.* **2018**, *8*, 2–10; c) T. Hune, S. Mamone, H. Schroeder, A. P. Jagtap, S. Sternkopf, G. Stevanato, S. Korchak, C. Fokken, C. A. Muller, A. B. Schmidt, D. Becker, S. Gloggler, *Chemphyschem* **2023**, *24*, e202200615; d) Y. Ding, S. Korchak, S. Mamone, A. P. Jagtap, G. Stevanato, S. Sternkopf, D. Moll, H. Schroeder, S. Becker, A. Fischer, E. Gerhardt, T. F. Outeiro, F. Opazo, C. Griesinger, S. Glöggler, *Chem.-Methods* **2022**, *2*(7), e202200023; e) M. Gierse, L. Nagel, M. Keim, S. Lucas, T. Speidel, T. Lobmeyer, G. Winter, F. Josten, S. Karaali, M. Fellermann, J. Scheuer, C. Muller, F. van Heijster, J. Skinner, J. Loffler, A. Parker, J. Handwerker, A. Marshall, A. Salhov, B. El-Kassem, C. Vassiliou, J. W. Blanchard, R. Picazo-Frutos, J. Eills, H. Barth, F. Jelezko, V. Rasche, F. Schilling, I. Schwartz, S. Knecht, *J. Am. Chem. Soc.* **2023**, *145*, 5960–5969; f) T. L. K. Hune, S. Mamone, A. B. Schmidt, I. Mahú, N. D'Apolito, D. Wiedermann, J. Brüning, S. Glöggler, *Appl. Magn. Reson.* **2023**, *54*, 1283–1295; g) S. Mamone, A. P. Jagtap, S. Korchak, Y. Ding, S. Sternkopf, S. Gloggler, *Angew. Chem. Int. Ed. Engl.* **2022**, *61*, e202206298; h) S. Korchak, S. Yang, S. Mamone, S. Gloggler, *ChemistryOpen* **2018**, *7*, 344–348; i) S. Korchak, S. Mamone, S. Glöggler, *ChemistryOpen* **2018**, *7*, 672–676; j) G. Stevanato, Y. Ding, S. Mamone, A. P. Jagtap, S. Korchak, S. Gloggler, *J. Am. Chem. Soc.* **2023**, *145*, 5864–5871; k) Y. Ding, G. Stevanato, F. von Bonin, D. Kube, S. Gloggler, *Chem. Sci.* **2023**, *14*, 7642–7647.

[11] M. S. Hossain, H. Karuniawati, A. A. Jairoun, Z. Urbi, J. Ooi, A. John, Y. C. Lim, K. M. K. Kibria, A. K. M. Mohiuddin, L. C. Ming, K. W. Goh, M. A. Hadi, *Cancers (Basel)* **2022**, *14*(7), 1732.

[12] P. Rawla, T. Sunkara, V. Gaduputi, *World J. Oncol.* **2019**, *10*, 10–27.

[13] J. Kleeff, M. Korc, M. Apte, C. La Vecchia, C. D. Johnson, A. V. Biankin, R. E. Neale, M. Tempero, D. A. Tuveson, R. H. Hruban, J. P. Neoptolemos, *Nat. Rev. Dis. Primers* **2016**, *2*, 16022.

[14] a) S. E. Bohndiek, M. I. Kettunen, D. E. Hu, K. M. Brindle, *Cancer Res.* **2012**, *72*, 854–864; b) Y. Saida, J. R. Brender, K. Yamamoto, J. B. Mitchell, M. C. Krishna, S. Kishimoto, *Cancer Res.* **2021**, *81*, 3693–3705.

[15] J. Sapi, L. Kovacs, D. A. Drexler, P. Kocsis, D. Gajari, Z. Sapi, *PLoS One* **2015**, *10*, e0142190.

[16] A. M. Funk, X. Wen, T. Hever, N. R. Maptue, C. Khemtong, A. D. Sherry, C. R. Malloy, *J Magn Reson* **2019**, *301*, 102–108.

[17] A. E. Hansen, H. Gutte, P. Holst, H. H. Johannesen, S. Rahbek, A. E. Clemmensen, M. M. E. Larsen, C. Schoier, J. Ardenkjaer-Larsen, T. L. Klausen, A. T. Kristensen, A. Kjaer, *Eur. J. Radiol.* **2018**, *103*, 6–12.

Manuscript received: January 16, 2024
Accepted manuscript online: June 18, 2024
Version of record online: ■■, ■■

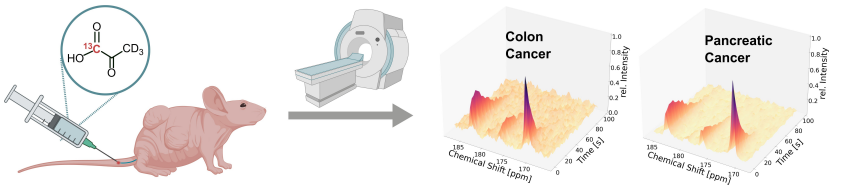

1-^{13}C-pyruvate-d_3 hyperpolarized via parahydrogen can be used to study altered metabolism with MRI in pancreatic as well as colon cancer human tumor-xenografts.

*L. M. Fries, T. L. K. Hune, S. Sternkopf, S. Mamone, K. L. Schneider, R. Schulz-Heddergott, D. Becker, S. Glöggler**

Real-Time Metabolic Magnetic Resonance Spectroscopy of Pancreatic and Colon Cancer Tumor-Xenografts with Parahydrogen Hyperpolarized 1-^{13}C Pyruvate-d_3